applied sciences

MDPI

Communication

Inspection of Semi-Elliptical Defects in a Steel Pipe Using the Metal Magnetic Memory Method

J. Jesús Villegas-Saucillo [1,*], Jose Javier Diaz-Carmona [1], Juan Prado-Olivares [1], Monserrat Sofia López-Cornejo [2], Ernesto A. Elvira-Hernández [3], Carlos A. Cerón-Álvarez [4] and Agustín L. Herrera-May [5,6,*]

1 Departamento de Ingeniería Eléctrica y Electrónica, Tecnológico Nacional de México en Celaya, Celaya 38020, Guanajuato, Mexico; javier.diaz@itcelaya.edu.mx (J.J.D.-C.); juan.prado@itcelaya.edu.mx (J.P.-O.)
2 Departamento Metal Mecánica, Tecnológico Nacional de México en Morelia, Morelia 58120, Michoacán, Mexico; monserrat.lc@morelia.tecnm.mx
3 Facultad de Ingeniería Mecánica y Ciencias Navales, Universidad Veracruzana, Boca del Río 94294, Veracruz, Mexico; eelvira@uv.mx
4 Facultad de Ingeniería Eléctrica y Electrónica, Universidad Veracruzana, Boca del Río 94294, Veracruz, Mexico; cceron@uv.mx
5 Micro and Nanotechnology, Reasearch Center, Universidad Veracruzana, Boca del Río 94294, Veracruz, Mexico
6 Maestría en Ingeniería Aplicada, Facultad de Ingeniería de la Construcción y el Hábitat, Universidad Veracruzana, Boca del Río 94294, Veracruz, Mexico
* Correspondence: jesus.villegas@itcelaya.edu.mx (J.J.V.-S.); leherrera@uv.mx (A.L.H.-M.)

Featured Application: Detection of superficial semi-elliptical defects in steel pipes using the variation in the self-magnetic flux leakage based on the metal magnetic memory method.

Abstract: Ferromagnetic pipes are widely used for fluid transportation in various industries. The failure of these ferromagnetic pipes due to surface defects can generate industrial accidents, economic losses, and environmental pollution. Non-destructive testing techniques are required to detect these surface defects. An alternative is the metal magnetic memory (MMM) method, which can be employed to detect surface flaws in ferromagnetic structures. Based on this method, we present an analysis of experimental results of the magnetic field variations around five different surface semi-elliptical defects of an ASTM A36 steel pipe. A measurement system of MMM signals is implemented with a rotatory mechanism, a magnetoresistive sensor, a data processing unit, and a control digital unit. The MMM method does not require expensive equipment or special treatment of the ferromagnetic structures. In order to research a potential relationship between the defect sample size and the measured MMM signals, variable defect dimensions are experimentally considered. According to these results, the shape and magnitude of the normal and tangential MMM signals are altered by the superficial semi-elliptical defects. In particular, the maximum and mean tangential components and the maximum and minimum normal components are related to the defect dimensions. The proposed measurement system can be used to study the behavior of magnetic field variations around surface defects of ferromagnetic pipes. This system can be adapted to measure the position and damage level of small defects on the surface of ferromagnetic pipes.

Keywords: ferromagnetic structure; surface magnetic defects; magnetic field sensor; metal magnetic memory method; non-destructive testing; magnetic field variation; semi-elliptic defect

Citation: Villegas-Saucillo, J.J.; Diaz-Carmona, J.J.; Prado-Olivares, J.; López-Cornejo, M.S.; Elvira-Hernández, E.A.; Cerón-Álvarez, C.A.; Herrera-May, A.L. Inspection of Semi-Elliptical Defects in a Steel Pipe Using the Metal Magnetic Memory Method. *Appl. Sci.* **2024**, *14*, 5308. https://doi.org/10.3390/app14125308

Academic Editor: Jacek Salach

Received: 24 April 2024
Revised: 7 June 2024
Accepted: 14 June 2024
Published: 19 June 2024

1. Introduction

Different liquids and gases are transported daily through steel pipes between industries and city installations. Efficient damage detection techniques in transportation ferromagnetic pipelines are required to avoid catastrophic accidents or environmental pollution. These accidents can generate high economic loss and damage to the human

population. For instance, the US has approximately 170,000 miles of hazardous liquid pipelines [1]. According to current regulations, hazardous liquids include petroleum, petroleum products, and anhydrous ammonia. About 66% of domestic petroleum moves through these pipelines [2]. The types of costs due to accidents involving US hazardous liquid pipeline infrastructure include the following: (i) the value of the product lost; (ii) public, private, and operator property damage; and (iii) cleanup, recovery, and other costs [3].

Damage detection in steel pipes is an essential challenge for non-destructive testing (NDT). Different NDT techniques have been employed for damage monitoring on ferromagnetic pipes, including liquid penetrant tests [4], ultrasonic tests [5], dynamic permeability testing [6], corrosion monitoring techniques [7], visual inspection and assessment techniques [8], eddy current testing [9], magnetic flux leakage testing [10], and X-ray inspection [11]. Defects in ferromagnetic pipes can be detected using liquid-penetrant testing based on the accumulation of a liquid around the defect on the sample surface. However, this NDT technique requires smooth and contaminant-free surfaces [12]. In ultrasonic testing, small defects in ferromagnetic pipes can be detected using ultrasonic pulses. Nonetheless, ultrasonic testing requires highly trained and experienced operators [13–15]. On the other hand, visual inspection NDT techniques can be employed to monitor pipe surface flaws [16,17]. Nevertheless, visual inspection is suitable for detecting relatively large ferromagnetic defects. In another NDT technique, the ferromagnetic pipe cracks can be detected using small magnetic particles through a dry or wet suspension of iron filings. However, this NDT technique has a low sensitivity of the inspection of cracks parallel to the applied magnetic field [18,19]. Another NDT technique is based on the eddy current, which can detect cracks in ferromagnetic pipelines [20,21]. This NDT technique requires an electromagnetic energy source for the eddy current induction on the pipe surface and high-skilled personnel to analyze the results. Moreover, magnetic flux leakage is another NDT technique for monitoring flaws in ferromagnetic pipes, in which the pipe is magnetized, employing an external magnetic field [22–24]. Finally, the X-ray inspection NDT can be used for monitoring surface or internal discontinuities in ferromagnetic pipes. However, this NDT technique requires high-cost equipment and skilled personnel [25].

Flaws on ferromagnetic pipes can be detected using conventional NDT techniques, although several NDT techniques require expensive specialized equipment and sample treatments. Furthermore, these NDT techniques require highly skilled personnel to study their results. Also, conventional NDT techniques have problems in monitoring early stage damage on ferromagnetic pipe surfaces, such as small defects at the micrometer scale and in stress concentration zones (SCZs) [26]. On the other hand, magnetic properties analysis has been used in NDT techniques to characterize ferromagnetic materials. For instance, the micromagnetic characterization of ferromagnetic steels in various heat treatment conditions can be measured using a hysteresis frame device [27]. Magnetic force microscopy can be employed to assess the magnetic properties of nanomaterials [28].

The metal magnetic memory (MMM) method is an NDT technique used to detect flaws in ferromagnetic structures and it was introduced by Duvov [29]. The MMM method is based on the magneto-elasticity property associated with the magnetic fields of ferromagnetic materials under stress as well as with the geomagnetic fields. The MMM method can measure the magnetic field shifts on ferromagnetic surfaces [30–37]. This method does not need artificial magnetic field sources, which is in contrast with magnetic flux leakage (MFL) testing [38–40]. In ferromagnetic materials, the magnetic field measured with the MMM method is related to the residual magnetic leakage field (RMFL) around surface defects [41–43].

The surface defects on ferromagnetic samples can be measured using the variations of the MMM signals around the defects without skilled personnel and expensive equipment [44,45]. The ferromagnetic materials may have residual magnetic fields due to their fabrication processes, flaws, SCZs, and applied magnetic fields. Small variations in the magnetic field around the surface defects of ferromagnetic structures can be measured by employing highly sensitive and high-resolution magnetometers. This MMM method can

detect flaws and SCZs on ferromagnetic structure surfaces. According to mathematical models reported by [46,47], the MMM signals around flaws on ferromagnetic surfaces register a tangential $H_t(x)$ component peak value and a normal $H_n(x)$ component zero value at the center of the ferromagnetic material defect or SCZ [48], as is depicted in Figure 1.

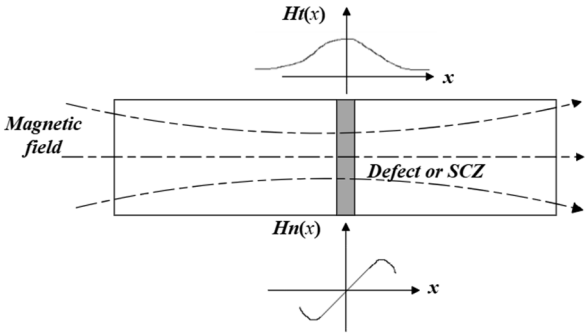

Figure 1. Theoretical results of the tangential and normal MMM signals around a defect or SCZ of a ferromagnetic sample.

The MMM method is used in diverse fields due to its easy and low-cost implementation. This method can assess the size and shape of the defects on a ferromagnetic pipe surface [34]. Various researchers have reported models and experimental tests to quantify the relationship between the defect size and the variation in their MMM signals [30–32,40,47,49]. Nevertheless, this method requires more experimental tests to quantify the shape and size of different defects on pipe surfaces. Herein, we report the analysis of the behavior of the MMM signals related to the size and shape of five different semi-elliptical defects on the surface of a ferromagnetic pipe. The MMM signals are measured using a rotatory structure, a magnetoresistive sensor, a microcontroller board, and a laptop. According to the experimental results, the size of semi-elliptical defects can be estimated by studying the behavior of the normal and tangential MMM signals. This measurement system of MMM signals can be used to predict the position and size of semi-elliptical defects on the surface of ferromagnetic pipes. This system does not require expensive equipment and highly skilled operators.

2. Materials and Methods

The measurement system for the ferromagnetic pipe sample is shown in Figure 2. An ATmega2560 microcontroller board (Arduino, Turin, Italy) is used for the data acquisition of the magnetic field sensor, actuator control, and data transmission to the computer. The data processing and MMM signals are plotted using MATLAB software (version 2022).

The MMM signals are measured with the three-axis magnetoresistive sensor MAG3110 (Freescale Semiconductor Inc., Austin, TX, USA) that is placed at a fixed distance of 2 mm from the pipe surface. The proposed system can measure the MMM signals of defects on the surface of ferromagnetic pipes in rotation using the one-step motor NEMA-17 (Leadshine Technology Co., Shenzhen, China) driven by the DVR8825 (Texas Instruents, Dallas, TX, USA) shield board. The data of the magnetoresistive sensor are transferred to a microcontroller board using I2C. Next, the data of this microcontroller board are transferred to a computer using USB. The structure of the measurement system was fabricated with non-magnetic materials, such as nylamid, copper, and aluminum. This system can be used for pipes with different diameters.

The pipe is collocated on the nylamid rotary disk that is driven by the x-axis step motor using a speed-reduction copper gear. This speed-reduction gear has internal and external diameters of 78.5 mm and 89 mm, respectively, a width of 5.5 mm, and a total of 102 teeth. A speed reduction from 1.8 degrees/step to 0.00227 degrees/step is achieved with the gear system, as shown in Figure 3.

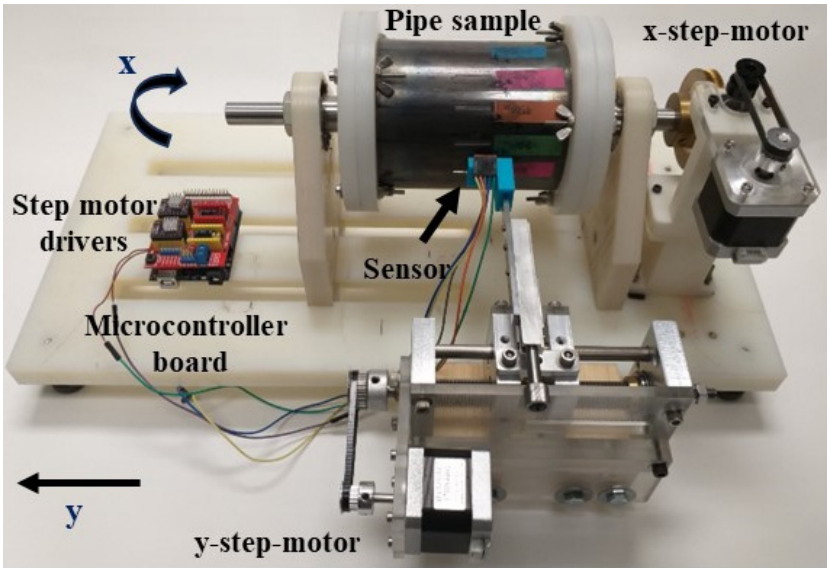

Figure 2. Measurement system of the MMM signals around semi-elliptical defects on the surface of a ferromagnetic pipe.

Figure 3. The gear system of the measurement system.

The control of the step motors for pipe movement and sensor data acquisition/transmission is achieved by the microcontroller program that is developed in the Arduino programming language. The rotational and longitudinal movements of the pipe are driven by the *x*-axis and *y*-axis step motors, respectively. Figure 4 depicts the program flowchart used to measure the MMM signals of the defects on the pipe surface. The main program is constantly pooling a command, which is serially received from the computer, to set a counterclockwise or clockwise pipe rotational movement. The pipe rotational angle is computed by an encoder value reading within an interrupt service routine (ISR). A counterclockwise command (N_Clk) is first received at the start of the scan. The sensor data, current degree, and arc length are serially sent to a computer within the counterclockwise scan until a reference angle is reached. Then, a clockwise scanning command is received (Clk), and the same information is serially sent until the initial position is reached. The data are serially received by the computer using the MATLAB software, in which the MMM signals are processed.

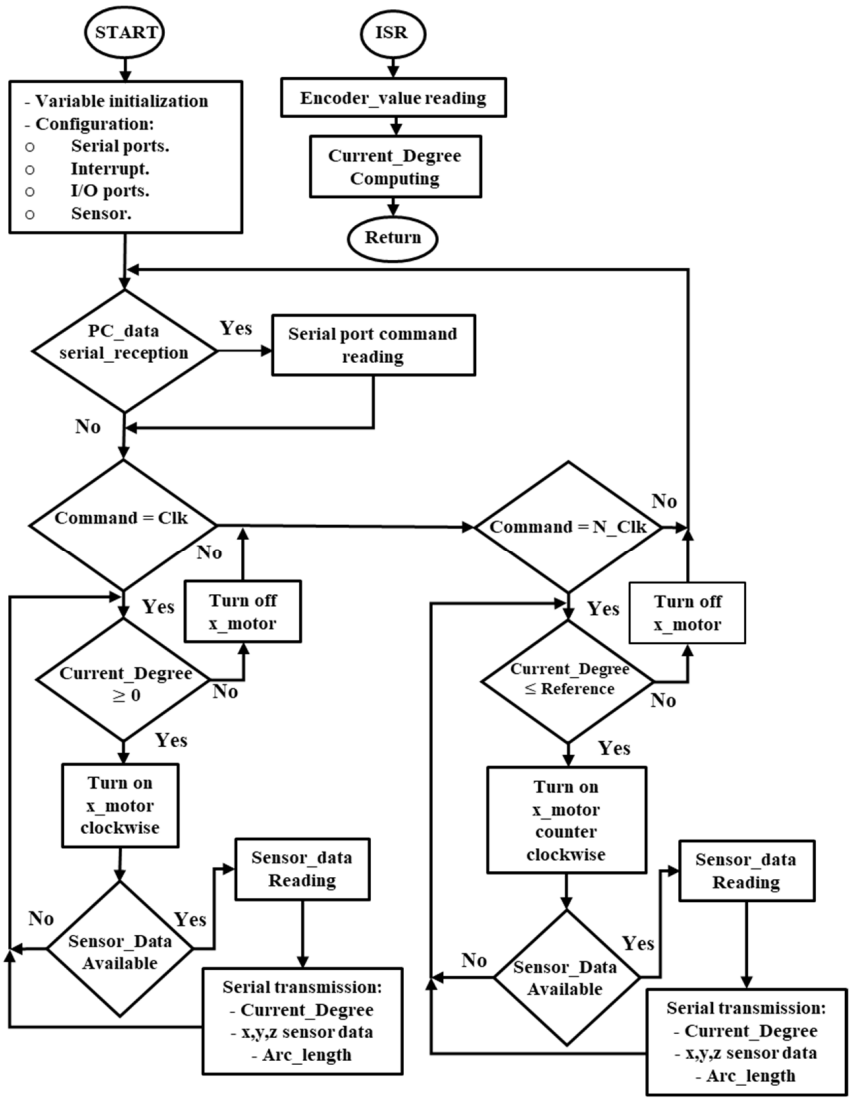

Figure 4. Flowchart of the measurement system of semi-elliptical defects in ferromagnetic pipes.

3. Results and Discussion

Five semi-elliptical shape defects were made on the surface of an ASTM A36 ferromagnetic pipe [50] with a length of 113.55 mm, an outer diameter of 89 mm, and a thickness of 5.45 mm. The defects were generated with the vertical cutter tool Ball Noise End Mills series 1725 through a computer numerical control (CNC) machine (see Figure 5). The resulting shape dimensions of the five defects are depicted in Figure 6.

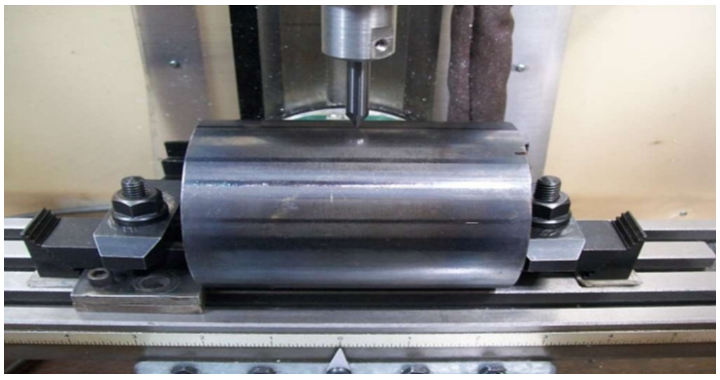

Figure 5. Generation of semi-elliptical shape defects on the pipe surface using the CNC machine.

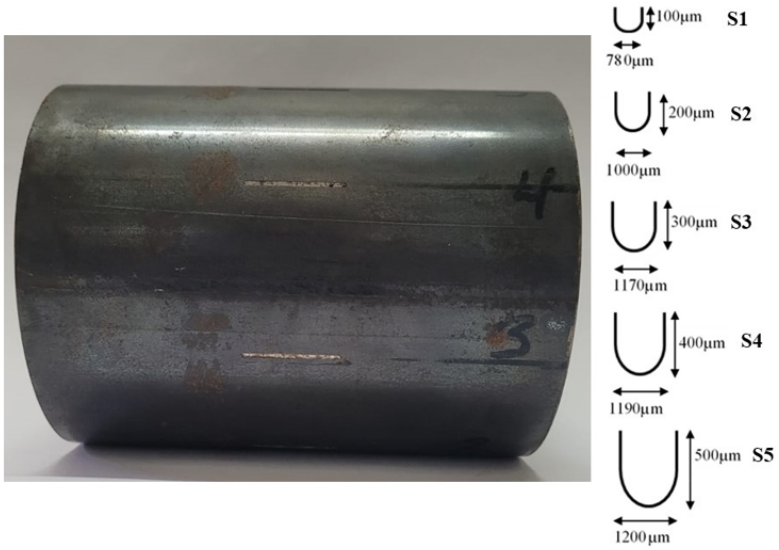

Figure 6. Dimensions of the five semi-elliptical defects machined on the surface of the ASTM A36 ferromagnetic pipe.

The tangential ($H_t(x)$) and normal ($H_n(x)$) MMM signals around semi-elliptical defects on the pipe surface were obtained using the measurement system. Six continuous tests were reported for each of the five semielliptical defects S1–S5. The scan length was 12 mm with the defect located in the center.

The tangential and normal MMM signals for the five defects are shown in Figures 7 and 8, respectively. As it is observed, the resulting MMM signal shapes for all the samples agree with the theoretically expected values; see Figure 1. The tangential component maximum $H_t\_max(x)$ and the tangential component mean value along the scanning length $H_t\_mean(x)$ are shown in Table 1. In addition, Table 2 shows the maximum and minimum values of the MMM signal component $H_n(x)\_max$ and $H_n(x)\_min$, the distance between the normal component maximum and minimum values $\Delta_n(x)$, and the normal component mean value along the scanning length $H_n(x)\_mean$.

Table 1. Tangential MMM signals of the five semi-elliptical defects.

Defect Sample	$H_t(x)\_max$ (mT)	$H_t(x)\_mean$ (mT)
S1	83.28 ± 0.354	43.49 ± 0.335
S2	91.3 ± 0.328	46.77 ± 0.265
S3	92.55 ± 0.243	56.66 ± 0.288
S4	86.12 ± 0.160	55.77 ± 0.237
S5	80.27 ± 0.207	57.42 ± 0.380

Table 2. Normal MMM signals of the five semi-elliptical defects.

Defect Sample	$H_n(x)\_min$ (mT)	$H_n(x)\_max$ (mT)	$\Delta_n(x)$ (mm)	$H_n(x)\_mean$ (mT)
S1	160.75 ± 0.596	217.15 ± 0.493	3.806 ± 0.242	183.72 ± 0.304
S2	194.2 ± 1.018	263.18 ± 0.564	3.526 ± 0.411	225.16 ± 0.448
S3	193.92 ± 0.728	260.67 ± 0.589	3.814 ± 0.885	223.16 ± 0.545
S4	188.55 ± 0.468	244.17 ± 0.516	2.115 ± 0.152	216.42 ± 0.127
S5	196.57 ± 0.398	237.15 ± 0.423	2.423 ± 0.128	220.15 ± 0.266

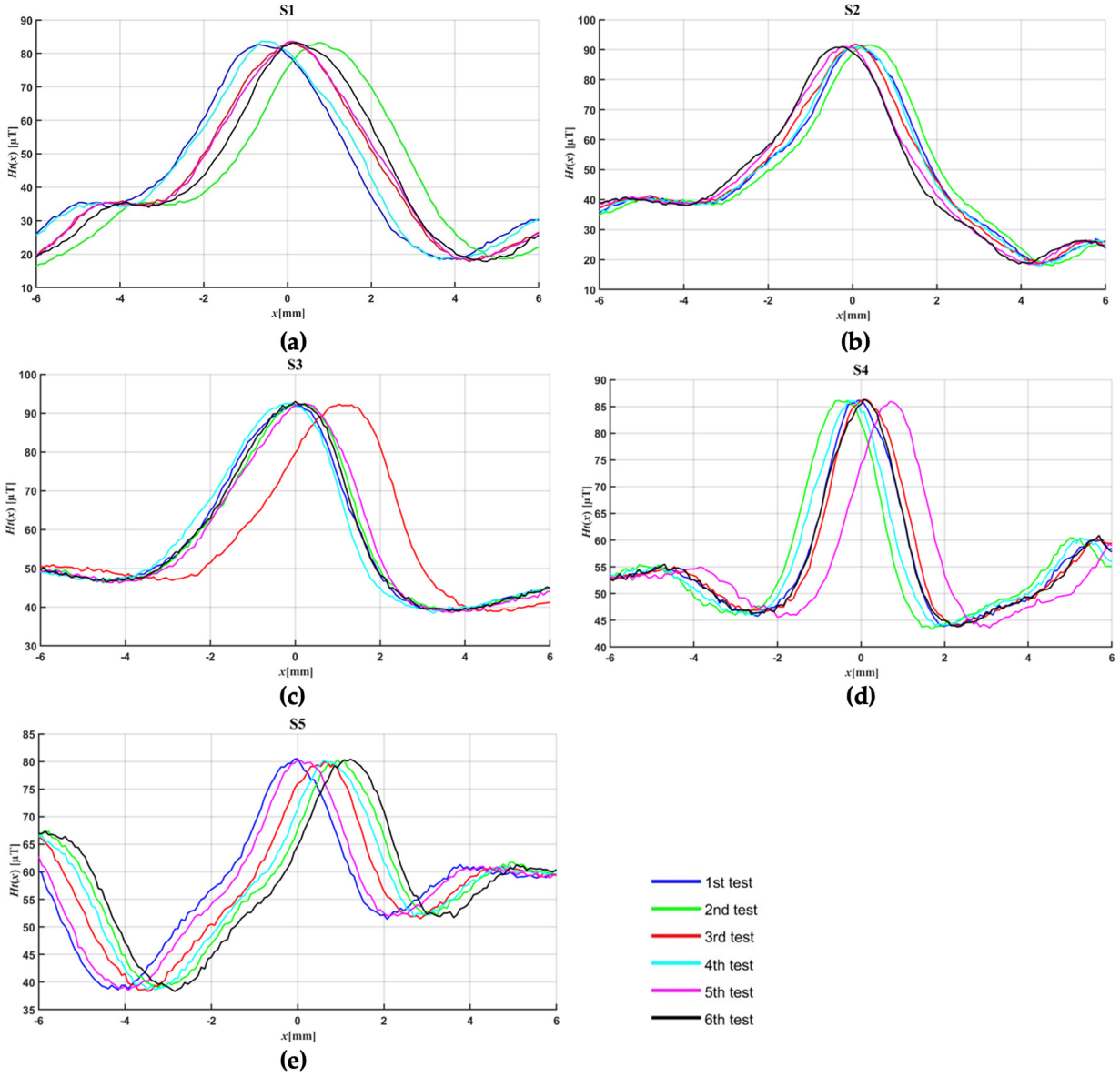

Figure 7. Tangential MMM signals around the semi-elliptical defects (**a**) S1, (**b**) S2, (**c**) S3, (**d**) S4, and (**e**) S5 of the ASTM A36 steel pipe.

The maximum tangential component $H_t(x)\_max$ has an increasing behavior for the defect samples S1, S2, and S3 and a decreasing behavior for S4 and S5. The tangential component mean $H_t(x)\_mean$ has an increasing value tendency from S1 to S5. In this sense, the measuring of $H_t(x)\_max$ and $H_t(x)\_mean$ might be further researched to be used to quantitatively determine the defect severity level. As it is observed in Figure 7, the location of the maximum tangential values are nearby the defect centers. Hence, such values might be used to locate a defect.

As can be seen from Table 2, no significant difference in the normal component mean value $H_n(x)\_mean$ was obtained for the considered defect samples. A higher value of the distance between the minimum and maximum normal component locations $\Delta_n(x)$ was achieved for S1, S2, and S3 compared with S4 and S5. Hence, the smaller the defect dimensions, the higher the distance $\Delta_n(x)$.

As it is observed for all five semi-elliptical defects samples, the peak value of the tangential component signal is located near the defect center (x = 0 mm). Moreover, the deepest defect has the highest tangential component mean value. On the other hand, the

normal component signal maximum and minimum values are located approximately near the defect edges.

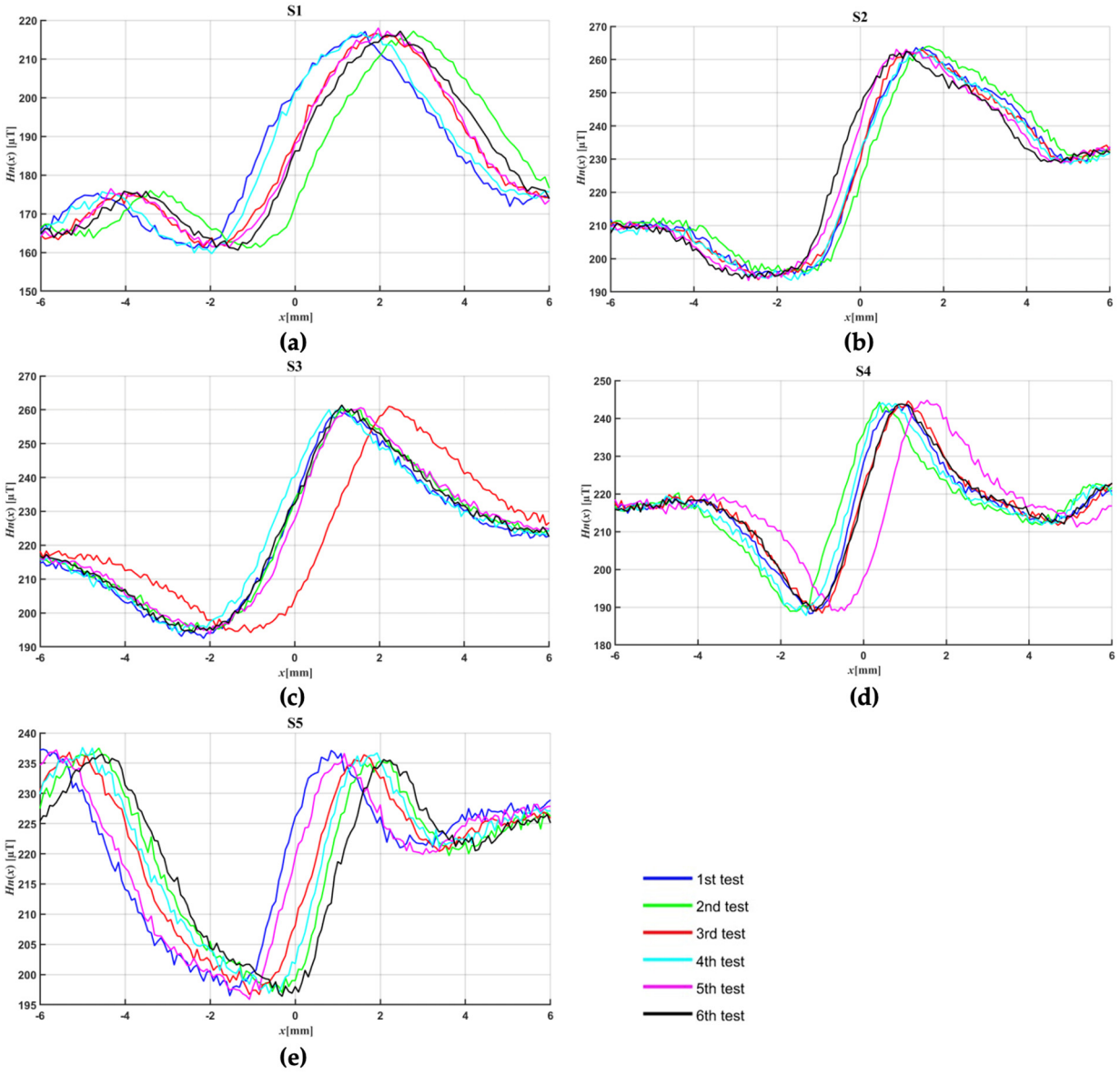

Figure 8. Normal MMM signals around the semi-elliptical defects (**a**) S1, (**b**) S2, (**c**) S3, (**d**) S4, and (**e**) S5 of the ASTM A36 steel pipe.

4. Conclusions

An MMM-based analysis of the magnetic field variations around five semi-elliptical defects with different sizes on an ASTM A36 steel pipe was reported. A measuring system not requiring high-cost equipment, highly skilled operators, and additional pipe treatment was implemented for monitoring MMM signals on the surface of ferromagnetic pipes. The characterized MMM normal and tangential component signals due to semi-elliptical defect dimensions were achieved by the measuring system.

The defect locations were discovered by using the measured MMM normal and tangential components in the experimental stage. Although the defects were completely located, further experimental work involving signal analysis techniques is required to quantitatively characterize the defect severity level, which is a promising future application of the measuring system. Based on the results of the MMM component signals, the maximum and mean tangential component values as well as the distance between the

location of the maximum and minimum normal component values were found to be related to the defect dimension. These results can be used in future research for a quantitative assessment of the defect severity level.

The described MMM signals measuring system is a helpful tool in researching NDT magnetic methods focused on analyzing defects or SCZs on ferromagnetic tubes. The effect analysis of measured MMM signal components due to defined defect shapes, stress concentration in specific pipe zones, and damage severity level is left as future work.

Author Contributions: Conceptualization, J.J.V.-S. and A.L.H.-M.; methodology, J.J.D.-C. and M.S.L.-C.; validation, J.J.V.-S.; investigation, E.A.E.-H., J.P.-O. and C.A.C.-Á.; writing—review and editing, A.L.H.-M. and J.J.D.-C. All authors have read and agreed to the published version of the manuscript.

Funding: This research was funded by Tecnológico Nacional de México grant number 16960.23-P and project title: "Diseño, construcción de un sistema embebido y una estructura de inspección para identificar la variación del campo magnético debido a discontinuidades geométricas en superficies de materiales ferromagnéticos por el método de memoria magnética de los metales (MMM)".

Institutional Review Board Statement: Not applicable.

Informed Consent Statement: Not applicable.

Data Availability Statement: Data is contained within the article.

Acknowledgments: This research was developed at "Universidad Veracruzana" and "Tecnológico Nacional de México Campus Celaya".

Conflicts of Interest: The authors declare no conflicts of interest.

References

1. Yuhua, D.; Datao, Y. Estimation of failure probability of oil and gas transmission pipelines by fuzzy fault tree analysis. *J. Loss Prev. Process Ind.* **2005**, *18*, 83–88. [CrossRef]
2. Dziubiński, M.; Frątczak, M.; Markowski, A.S. Aspects of risk analysis associated with major failures of fuel pipelines. *J. Loss Prev. Process Ind.* **2006**, *19*, 399–408. [CrossRef]
3. Restrepo, C.E.; Simonoff, J.S.; Zimmerman, R. Causes, cost consequences, and risk implications of accidents in US hazardous liquid pipeline infrastructure. *Int. J. Crit. Infrastruct. Prot.* **2009**, *2*, 38–50. [CrossRef]
4. Vera, J.; Caballero, L.; Taboada, M. Reliability of Dye Penetrant Inspection Method to Detect Weld Discontinuities. *Russ. J. Nondestruct. Test.* **2024**, *60*, 85–95. [CrossRef]
5. Fan, Z.; Bai, K.; Chen, C. Ultrasonic testing in the field of engineering joining. *Int. J. Adv. Manuf. Technol.* **2024**, *132*, 4135–4160. [CrossRef]
6. Zhengyu, O.; Cheng, X.; Zandong, H.; Jisong, C.; Shihao, D. Nondestructive testing method for internal defects in ferromagnetic materials under weak bias magnetization. *Measurement* **2024**, *226*, 114173. [CrossRef]
7. Olsen, A.A. Corrosion Monitoring and Non-destructive Testing. In *Equipment Conditioning Monitoring and Techniques*; Springer: Cham, Switzerland, 2024. [CrossRef]
8. Gdoutos, E.; Konsta-Gdoutos, M. Nondestructive Testing (NDT). In *Mechanical Testing of Materials*; Solid Mechanics and Its Applications; Springer: Cham, Switzerland, 2024; Volume 275. [CrossRef]
9. Nadzri, N.; Saari, M.M.; Zaini MA, H.P.; Aziz, Z.A. Detection of vertical and horizontal crack in steel structure using a circular eddy current testing probe. In Proceedings of the AIP Conference Proceedings, Pahang, Malaysia, 5–6 December 2022; Volume 2998, p. 060010. [CrossRef]
10. Shen, Y.; Wang, Y.; Wu, B.; Li, P.; Han, Z.; Zhang, C.; Liu, X. A novel sensor based on the composite mechanism of magnetic flux leakage and magnetic field disturbance for comprehensive inspection of defects with varying angles and widths. *NDT E Int.* **2024**, *145*, 103131. [CrossRef]
11. Hassan, O.S.; Rahman, M.S.; Mustapha, A.A.; Gaya, S.; Abou-Khousa, M.A.; Cantwell, W.J. Inspection of antennas embedded in smart composite structures using microwave NDT methods and X-ray computed tomography. *Measurement* **2024**, *226*, 114086. [CrossRef]
12. Lu, Q.Y.; Wong, C.H. Applications of non-destructive testing techniques for post-process control of additively manufactured parts. *Virtual Phys. Prototyp.* **2017**, *12*, 301–321. [CrossRef]
13. Khalili, P.; Cawley, P. The choice of ultrasonic inspection method for the detection of corrosion at inaccessible locations. *NDT E Int.* **2018**, *99*, 80–92. [CrossRef]
14. Zhou, Y.L.; Quian, X.; Birnie, A.; Zhao, X.-L. A reference free ultrasonic phased array to identify surface cracks in welded steel pipes based on transmissibility. *Intern. J. Press. Vessels Pip.* **2018**, *168*, 66–78. [CrossRef]

15. Li, X.; Wang, Y.; Wan, X.; Tang, B.; Qin, Y.; Xu, C. Physics-informed deep filtering of ultrasonic guided waves for incipient defect inspection of large-scale square tube structures. *J. Sound Vib.* **2023**, *567*, 118066. [CrossRef]
16. Wang, G.; Tse, P.W.; Yuan, M. Automatic internal crack detection from a sequence of infrared images with a triple-threshold Canny edge detector. *Meas. Sci. Technol.* **2018**, *29*, 025403. [CrossRef]
17. Manjunatha, M.; Selvakumar, A.A.; Godeswar, V.P.; Manimaran, R. A low cost underwater robot with grippers for visual inspection of external pipeline surface. *Proc. Comp. Sci.* **2018**, *133*, 108–115. [CrossRef]
18. Kordonski, W.; Gorodkin, S.; Behlok, R. In-line monitoring of (MR) fluid properties. *J. Magn. Magn. Mater.* **2015**, *382*, 328–334. [CrossRef]
19. Hajibagheri, H.R.; Heidari, A.; Amini, R. An experimental investigation of the nature of longitudinal cracks in oil and gas transmission pipelines. *J. Alloys Comp.* **2018**, *741*, 1121–1129. [CrossRef]
20. Zhang, W.; Shi, Y.; Li, Y.; Luo, Q. A Study of Quantifying Thickness of Ferromagnetic Pipes Based on Remote Field Eddy Current Testing. *Sensors* **2018**, *18*, 2769. [CrossRef]
21. Saffiudeen, M.F.; Syed, A.; Mohammed, F.T. Failure Analysis of Heat Exchanger Using Eddy Current Testing (ECT). *J. Fail. Anal. Prev.* **2023**, *23*, 1898–1906. [CrossRef]
22. Zhang, S.; Li, H.; Zhao, C. Defect-depth-field algorithm for simulating magnetic flux leakage signals based on discrete magnetic dipole model. *NDT E Intern.* **2023**, *139*, 102939. [CrossRef]
23. Liu, B.; Wu, Z.; Wang, P.; He, L.; Yang, L.; Lian, Z.; Liu, T. Quantization of magnetic flux leakage internal detection signals for composite defects of gas and oil pipelines. *Energy Rep.* **2023**, *9*, 5899–5914. [CrossRef]
24. Feng, B.; Yang, Y.; Sun, Y.; Deng, Z. Magnetization time lag caused by Eddy currents and its influence on high-speed magnetic flux leakage testing. *Res. Nondestruct. Eval.* **2019**, *30*, 189–204. [CrossRef]
25. Senck, S.; Scheerer, M.; Revol, V.; Plank, B.; Hannesschläger, C.; Gusenbauer, C.; Kastner, J. Microcrack characterization in loaded CFRP laminates using quantitative two- and three-dimensional X-ray dark-field imaging. *Compos. Part A Appl. Sci. Manuf.* **2018**, *115*, 206–214. [CrossRef]
26. Shi, P.; Jin, K.; Zheng, X. A magnetomechanical model for the magnetic memory method. *Intern. J. Mech. Sci.* **2017**, *124–125*, 229–241. [CrossRef]
27. Ankener, W.; Böttger, D.; Smaga, M.; Gabi, Y.; Strass, B.; Wolter, B.; Beck, T. Micromagnetic and Microstructural Characterization of Ferromagnetic Steels in Different Heat Treatment Conditions. *Sensors* **2022**, *22*, 4428. [CrossRef]
28. Winkler, R.; Ciria, M.; Ahmad, M.; Plank, H.; Marcuello, C. A Review of the Current State of Magnetic Force Microscopy to Unravel the Magnetic Properties of Nanomaterials Applied in Biological Systems and Future Directions for Quantum Technologies. *Nanomaterials* **2023**, *13*, 2585. [CrossRef]
29. Dubov, A.A. A study of metal properties using the method of magnetic memory. *Met. Sci. Heat Treat.* **1997**, *39*, 401–405. [CrossRef]
30. Villegas-Saucillo, J.J.; Díaz-Carmona, J.J.; Escarola-Rosas, M.A.; Vázquez-Leal, H.; Martínez-Castillo, J.; Herrera-May, A.L. Measurements of the Magnetic Field Variations Related with the Size of V-Shaped Notches in Steel Pipes. *Appl. Sci.* **2021**, *11*, 3940. [CrossRef]
31. Yao, K.; Deng, B.; Wang, Z.D. Numerical studies to signal characteristics with the metal magnetic memory-effect in plastically deformed samples. *NDT E Int.* **2012**, *47*, 7–17. [CrossRef]
32. Shi, P.; Jin, K.; Zhang, P.; Xie, S.; Chen, Z.; Zheng, X. Quantitative inversion of stress and crack in ferromagnetic materials based on metal magnetic memory method. *IEEE Trans. Magn.* **2018**, *54*, 6202011. [CrossRef]
33. Liu, B.; Ma, Z.; He, L.; Wang, D.; Zhang, H.; Ren, J. Quantitative study on the propagation characteristics of MMM signal for stress international detection of long distance oil and gas pipeline. *NDT E Int.* **2018**, *100*, 40–47. [CrossRef]
34. Villegas-Saucillo, J.J.; Díaz-Carmona, J.J.; Cerón-Álvarez, C.A.; Juárez-Aguirre, R.; Domínguez-Nicolás, S.M.; López-Huerta, F.; Herrera-May, A.L. Measurement System of Metal Magnetic Memory Method Signals around Rectangular Defects of a Ferromagnetic Pipe. *Appl. Sci.* **2019**, *9*, 2695. [CrossRef]
35. Dubov, A.; Kolokolniko, S. The metal magnetic memory method application for online monitoring of damage development in steel pipes and welded joints specimens. *Weld. World* **2013**, *57*, 123–136. [CrossRef]
36. Dubov, A.; Dubov, A.; Kolokolnikov, S. Detection of local stress concentration zones in engineering products-the lacking link in the non-destructive testing system. *Weld. World* **2018**, *62*, 301–309. [CrossRef]
37. Xu, K.; Qiu, X.; Tian, X. Theoretical investigation of metal magnetic memory testing technique for detection of magnetic flux leakage signals from buried defect. *Nondestruct. Test. Eval.* **2018**, *33*, 45–55. [CrossRef]
38. Shi, P.; Jin, K.; Zheng, X. A general nonlinear magnetomechanical model for ferromagnetic materials under a constant weak magnetic field. *J. Appl. Phys.* **2016**, *119*, 145103. [CrossRef]
39. Kolokolnikov, S.; Dubov, A.; Steklov, O. Assessment of welded joints stress-strain state inhomogeneity before and after post weld heat treatment based on the metal magnetic memory method. *Weld. World* **2016**, *64*, 665–672. [CrossRef]
40. Li, Z.; Dixon, S.; Cawley, P.; Jarvis, R.; Nagy, P.B.; Cabeza, S. Experimental studies of the magneto-mechanical memory (MMM) technique using permanently installed magnetic sensor arrays. *NDT E Int.* **2017**, *92*, 136–148. [CrossRef]
41. Yang, L.J.; Liu, B.; Chen, L.J.; Gao, S.W. The quantitative interpretation by measurement using the magnetic memory method (MMM)-based on density functional theory. *NDT E Int.* **2013**, *55*, 15–20. [CrossRef]
42. Dubov, A.A. Development of a metal magnetic memory method. *Chem. Petrol Eng.* **2012**, *47*, 837–839. [CrossRef]

43. Yao, K.; Wang, Z.D.; Deng, B.; Shen, K. Experimental research on metal magnetic memory method. *Exp. Mech.* **2012**, *52*, 305–314. [CrossRef]
44. Dubov, A.; Kolokolnikov, S. Assessment of the material state of oil and gas pipelines based on the metal magnetic memory method. *Weld. World* **2012**, *56*, 11–19. [CrossRef]
45. de Oca-Mora, N.J.M.; Woo-García, R.M.; Sánchez-Vidal, A.; Galván-Martínez, R.; Orozco-Cruz, R.; Carmona-Hernández, A.; Herrera-May, A.L.; Restrepo, J.; Algredo-Badillo, I.; López-Huerta, F. Simulation and Detection of Rectangular Magnetic Cracks in Metallic Plates. *J. Nondestruct. Eval.* **2023**, *42*, 19. [CrossRef]
46. Edwards, C.; Palmer, S.B. The magnetic leakage field of suface-beaking cacks. *J. Phys. D Appl. Phys.* **1986**, *19*, 657. [CrossRef]
47. Trevino, D.A.G.; Dutta, S.M.; Ghorbel, F.H.; Karkoub, M. An Improved Dipole Model of 3-D Magnetic Flux Leakage. *IEEE Trans. Magn.* **2016**, *52*, 6201707. [CrossRef]
48. Zhang, H.; Qiu, J.; Xia, R.; Cheng, C.; Zhou, J.; Jiang, H.; Li, Y. Corrosion damage evaluation of loaded steel strand based on self-magnetic flux leakage. *J. Magn. Magn. Mater.* **2021**, *549*, 168998. [CrossRef]
49. Pengpeng, S.; Xiaojing, Z. Magnetic charge model for 3D MMM signals. *Nondestruct. Test. Eval.* **2015**, *31*, 45–60. [CrossRef]
50. *A36/A36M-19*; Standard Specification for Carbon Structural Steel. ASTM International: West Conshohocken, PA, USA, 2019.